

**International Journal of Computational Materials Science and Surface Engineering**

ISSN online: 1753-3473 - ISSN print: 1753-3465

<https://www.inderscience.com/ijcmsse>

---

**Numerical simulation of SiC crystal growth during physical vapour transport using the lattice Boltzmann - phase field model**

Hu Zhao, Shilin Mao, Hui Xing, Dongke Sun

**DOI:** [10.1504/IJCMSSE.2023.10059324](https://doi.org/10.1504/IJCMSSE.2023.10059324)

**Article History:**

Received:	01 May 2023
Last revised:	15 May 2023
Accepted:	15 May 2023
Published online:	08 January 2024

# Numerical simulation of SiC crystal growth during physical vapour transport using the lattice Boltzmann – phase field model

---

Hu Zhao and Shilin Mao

School of Mechanical Engineering,  
Southeast University,  
Nanjing, 211189, China  
Email: zhao\_hu@seu.edu.cn  
Email: shilinmao@seu.edu.cn

Hui Xing

Research & Development Institute of Northwestern  
Polytechnical University in Shenzhen,  
Shenzhen, 518000, China  
Email: huixing@nwpu.edu.cn

Dongke Sun\*

School of Mechanical Engineering,  
Southeast University,  
Nanjing, 211189, China  
Email: dksun@seu.edu.cn  
\*Corresponding author

**Abstract:** The lattice Boltzmann-phase field (LB-PF) model is utilised to investigate SiC crystal growth in physical vapour transport (PVT). In the model, the magnetic vector potential equation is used to compute the magnetic field distribution of the growth environment, the thermal stress equation based on displacement is applied to solve the stress evolution in the crystals and the LB-PF equation is applied to describe the crystal growth. After model validation, the model is applied to study the temperature evolution and crystal growth under different coil positions, currents and pressures. The results show that moving up coils and increasing currents have little effect on axial temperature gradient in growth environment, the crystal growth rates could be increased by reducing the pressure. The present model has been demonstrated its potential in simulations of SiC crystal growth.

**Keywords:** SiC; crystal growth; lattice Boltzmann; phase field; physical vapour transport; stress; pressure.

**Reference** to this paper should be made as follows: Zhao, H., Mao, S., Xing, H. and Sun, D. (2023) 'Numerical simulation of SiC crystal growth during physical vapour transport using the lattice Boltzmann – phase field model', *Int. J. Computational Materials Science and Surface Engineering*, Vol. 11, Nos. 3/4, pp.253–271.

**Biographical notes:** Hu Zhao is a Master's student in the School of Mechanical Engineering, Southeast University, Nanjing, Jiangsu Province, China, and his main research interests are mesoscopic numerical simulation of complex systems.

Shilin Mao is a PhD student at the School of Mechanical Engineering, Southeast University, Nanjing, Jiangsu Province, China, with a research interest in numerical simulation of alloy solidification and dendrite growth.

Hui Xing is an Associate Professor in the School of Physical Science and Technology at Northwestern Polytechnical University in Xi'an, Shaanxi Province, China, where he received his PhD in computational materials science, crystal growth, and artificial intelligence.

Dongke Sun is a Professor in the School of Mechanical Engineering, Southeast University, Nanjing, Jiangsu Province, China. He has been focusing on modelling and simulation of solidification processes for a long time, and has been conducting research on melt flow, dendrite growth, thermal mass transport and defect formation in solidification processes, and has successfully combined phase field methods, metacellular automata methods and lattice Boltzmann methods and applied them to the study of convective heat transfer and microstructure formation laws in metal melts.

---

## 1 Introduction

The SiC with wide-bandgap, high thermal conductivity and high carrier saturation drift rate has great potential in high temperature, high frequency and intense radiation resistance (Kimoto, 2016). Preparation of SiC crystals by PVT is one of the most widely used techniques in recent years (Li et al., 2011; Wellmann, 2018). However, severe constraints exist on experimental measurements of SiC by high temperature, harsh environment and opaque crucible wall, it becomes more difficult to determine the appropriate process parameters for growing high quality crystals through experiments. Numerical simulation has become a research technology of SiC crystal growth, effectively reducing the time as well as the economic cost of traditional experimental methods (Ariyawong et al., 2015; Ha and Jeong, 2022).

To understand the heat transfer in SiC sublimation growth process. Yang et al. (2018a) established a three-dimensional numerical simulation platform for SiC crystals. The temperature and magnetic equations were discretised by using the finite volume method (FVM). The influences of coil structures on the temperature and temperature gradient in the growth environment were quantitatively analysed. The results showed that the spiral coil caused the non-axisymmetric temperature field. Su et al. (2014) established a two-dimensional model to study the influences of induction heating on the temperature field by using the finite element method (FEM), investigated the influences of different coil radii and frequencies on the temperature distribution and growth rates. The results showed that when the coil radius was in the range of 0.11–0.13 m and the frequency was in the range of 30 kHz to 40 kHz were good for crystal growth in the simulations. However, the influence of the flow field are not considered in the above researches. Later, Yan et al. (2014) calculated the flow and concentration field in the improved thermal design environment by using the FVM. The results showed that the crystal yield

can be increased by improving the crystal growth interface. However, the above research mainly focused on the growth of small size SiC crystals and ignored the influences of natural convection and Stefan flow. When the size of the growth device increased, the natural convection and Stefan effect could not be ignored. Therefore, it is necessary to analyse the heat transfer in the growth of large size SiC crystals.

To understand the formation mechanism and influencing factors of thermal stress in SiC crystals. Yang et al. (2018b) studied the temperature gradient and thermal stress evolution caused by different crucible structures. The results showed that the change of structure had a good effect on the radial and axial temperature gradients. Yang et al. (2012) studied the influences of different growth interface shapes on the thermal stress generation by using anisotropic elasticity method. Kim et al. (2012) investigated the effects of growth temperature and surface area on the thermal stress of SiC single crystals by using the FEM. The results showed that the wafers with higher thermal stress had lower crystallinity and more defects. However, the influences of crucible structures or crystal shapes on thermal stress of crystals are only considered in the above studies, the influence of the interaction between crucible and crystal on thermal stress generation is not considered.

To understand the morphologies and influencing factors of SiC crystal growth. Chaussende et al. (2009) obtained the nucleation and growth processes of 3C-SiC crystals by using the scanning electron microscopy (SEM) under experimental conditions and analysed the main difficulties associated with the growth of 3C-SiC single crystals. Geiser and Irle (2011) studied the microscopic growth of SiC crystals. The initial reaction of SiC on the c plane was simulated by atomic quantum chemical molecular dynamics based on the density functional method. Tokuda et al. (2014) used high temperature gas source method to study the SiC crystal growth. The results showed that in the absence of dendrite crystals, high temperature gradients were needed to achieve high volume growth. Secondly, high speed volume growth was achieved under high temperature gradient. However, the morphologies of SiC crystals during the SiC sublimation growth are only considered in the above studies, the interaction between macroscopic temperature field of SiC crystals and the crystal growth morphology has not been studied.

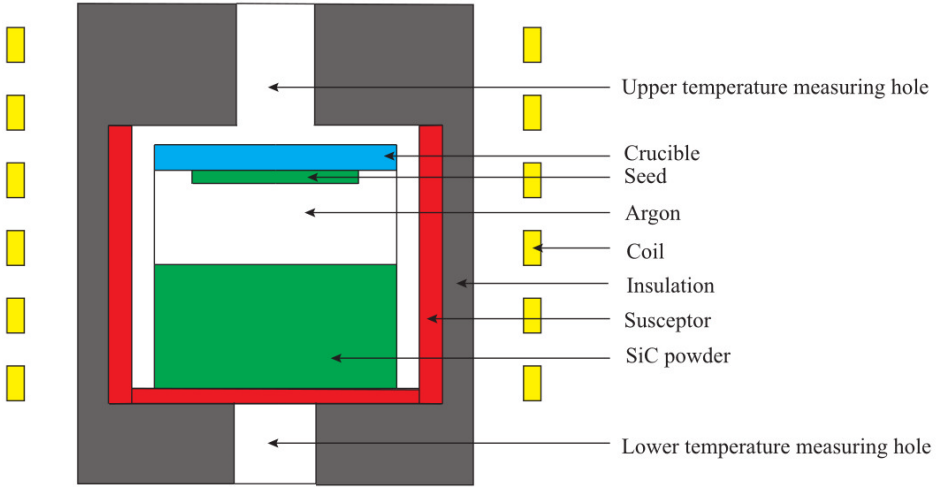
It has been proved that numerical simulation of crystal growth has a high guiding significance for the experimental preparation of SiC crystals. However, most of the methods have some limitations in calculation and the computational efficiency is relatively low. The LB-PF method is widely used to simulate heat transfer and crystal growth because of its simple algorithm, easy implementation and effective solution of partial differential equations.

The aim of this paper is to establish a LB-PF model to study the growth of SiC crystals in PVT. Briefly, the rest of the paper is organised as follows. Section 2 gives the detailed description of the model, which includes heat transfer, thermal stress generation and crystal growth. Section 3 presents the validations and simulations of the model. Firstly, the reliability of the model is quantitatively validated by simulating thermal stress generation in the cantilever beam. Next, the growth of crystals is qualitatively validated by simulation. Then, the effects of current and coil position on the temperature distribution of SiC crystals are studied. Moreover, the effects of dimensionless temperature and pressure variation rates on the crystal growth are investigated. Finally, the conclusion is presented in Section 4.

## 2 Mathematical model

Figure 1 shows a typical device of SiC crystal growth in PVT. The growth device consists of crucible, insulation, argon, powder, susceptor and coil. The SiC powder is placed in the crucible and heated by induction heating, the seed is attached to the bottom of the crucible lid.

**Figure 1** The schematic diagram of SiC crystal growth device in PVT (see online version for colours)



### 2.1 Modelling of convective heat transfer and thermal stress generation

#### 2.1.1 Modelling of induction heating

The magnetic field is obtained by solving the magnetic potential vector equation. It is assumed that all the mediums are linear and isotropic, and the displacement current is neglected in the calculation of induction heating. The equation for magnetic potential vector can be written as (Su et al., 2014)

$$\nabla \times \left( \frac{1}{\mu_m} \nabla \times \mathbf{A} \right) + \epsilon_m \frac{\partial^2 \mathbf{A}}{\partial t^2} + \sigma_1 \frac{\partial \mathbf{A}}{\partial t} = \mathbf{J}_{Coil}, \quad (1)$$

where  $\mathbf{A}$  is magnetic potential vector,  $\mu_m$  is magnetic permeability,  $\epsilon_m$  is electrical permittivity,  $\sigma_1$  is electrical conductivity, and  $\mathbf{J}_{coil}$  represents coil current density. The magnetic potential vector  $\mathbf{A}$  is calculated by

$$\mathbf{A} = A_r + iA_i, \quad (2)$$

where the real part  $A_r$  is referred to as in-phase component and the imaginary part  $A_i$  is termed as out-of-phase component (Ma et al., 2003). In the SiC crystal growth device, the boundary conditions are

$$A_r = 0, \quad A_i = 0, \quad \text{at } r = 0 \text{ and } (r^2 + z^2) \rightarrow \infty \quad (3)$$

### 2.1.2 Modelling of incompressible gas flows

The influences of natural convection and Stefan flow on the gas components transport are considered during the growth of SiC crystals. It is assumed that the gas phase components are ideal gases and do not react with each other. The gas flows in the SiC sublimation growth can be expressed by the Navier-Stokes (N-S) equations as follows (Chen et al., 2007)

$$\nabla \cdot (\rho \mathbf{u}) = 0, \quad (4)$$

$$\rho \left[ \frac{\partial \mathbf{u}}{\partial t} + (\mathbf{u} \cdot \nabla) \mathbf{u} \right] = -\nabla p + \mu \nabla^2 \mathbf{u} + \mathbf{F}, \quad (5)$$

where  $\rho$  is density,  $\mathbf{u}$  is velocity,  $p$  is pressure,  $\mu$  is dynamic viscosity, and  $\mathbf{F}$  represents thermal buoyancy. Based Boussinesq's approximation, the thermal buoyancy  $\mathbf{F}$  is

$$\mathbf{F} = -\rho \mathbf{g} \alpha (T - T_0), \quad (6)$$

where  $\mathbf{g}$  denotes acceleration of gravity,  $\alpha$  represents volume thermal expansion coefficient, and  $T_0$  is ambient temperature.

The Hertz-Knudsen equation (Chen et al., 2001) for crystal growth is introduced to describe the fluid boundary conditions. On the surface of SiC powder,

$$p|_{z=\text{surface}} = p^* (T_{\text{max}}) \quad (7)$$

Crucible wall boundary conditions,

$$u|_{\text{wall}} = v|_{\text{wall}} = 0, \quad \frac{\partial^2 p}{\partial r^2}|_{\text{wall}} = 0, \quad (8)$$

where  $u$  and  $v$  are the axial and radial velocities, respectively. Axis of boundary condition,

$$\frac{\partial u}{\partial t} = 0, \quad \frac{\partial p}{\partial r} = 0, \quad \text{at } r = 0. \quad (9)$$

### 2.1.3 Modelling of convective heat transfer

The temperature is calculated using the energy transport equation under the effects of heat conduction, convection and radiation. It is assumed that each surface in the radiation heat transfer is a diffuse grey surface. The convective heat transfer can be described by the following energy equation (Liu et al., 2008)

$$(\rho C_p)_{\text{eff}} \frac{\partial T}{\partial t} + \rho C_{p,f} \mathbf{u} \cdot \nabla T = \nabla \cdot (\kappa_{\text{eff}} \nabla T) + Q_{rc} + Q_s, \quad (10)$$

where  $\rho_{\text{eff}}$  denotes equivalent density,  $(C_p)_{\text{eff}}$  denotes equivalent specific heat capacity,  $T$  is temperature,  $C_{p,f}$  is fluid specific heat capacity,  $\kappa_{\text{eff}}$  denotes equivalent thermal conductivity,  $Q_{rc}$  represents heat source term acting on the wall, such as radiation and convection heat exchange on the insulation and crucible wall, and  $Q_s$  represents induction heating source term. The  $Q_s$  can be obtained by using the following expression

$$Q_s = \frac{1}{2} \sigma (2\pi f)^2 (A_r^2 + A_i^2) \quad (11)$$

A coupled convection-radiation boundary condition is applied on the outer surface of the susceptor and insulation

$$-\kappa \frac{\partial T}{\partial n} = h(T - T_\infty) + \varepsilon \sigma (T^4 - T_\infty^4) \tag{12}$$

where  $\kappa$  represents thermal conductivity of the material,  $\mathbf{n}$  is vector normal to outer surface of the susceptor and insulation,  $h$  denotes convective heat transfer coefficient between insulation and outside air,  $T_\infty$  is environment temperature,  $\varepsilon$  is material surface emissivity, and  $\sigma$  denotes Stefan-Boltzmann constant.

The axial boundary condition is set as

$$\frac{\partial T}{\partial r} = 0, \quad \text{at } r = 0. \tag{13}$$

### 2.1.4 Modelling of thermal stress generation

In the macroscopic coordinate used for stress calculations, the top of the crucible lid is set to  $z = 0$ . The magnitude of gravity in seed is negligible compared to the thermal stress, which is not considered in the equilibrium equations. The thermoelastic crystals satisfy the following equilibrium equations (Chen et al., 2010)

$$\frac{1}{r} \frac{\partial}{\partial r} (r \sigma_{rr}) + \frac{\partial \tau_{rz}}{\partial z} - \frac{\sigma_{\varphi\varphi}}{r} = 0, \tag{14}$$

$$\frac{1}{r} \frac{\partial}{\partial r} (r \tau_{rz}) + \frac{\partial \sigma_{zz}}{\partial z} = 0, \tag{15}$$

where  $\sigma_{rr}$ ,  $\sigma_{zz}$  and  $\sigma_{\varphi\varphi}$  are the normal stress components in the radial, axial and azimuthal directions, respectively, and  $\tau_{rz}$  is the shear stress.

The stress-strain relationship can be expressed as follows (Yang et al., 2022)

$$\begin{pmatrix} \sigma_{rr} \\ \sigma_{\varphi\varphi} \\ \sigma_{zz} \\ \sigma_{rz} \end{pmatrix} = \begin{pmatrix} c_{11} & c_{12} & c_{13} & 0 \\ c_{12} & c_{22} & c_{23} & 0 \\ c_{13} & c_{23} & c_{33} & 0 \\ 0 & 0 & 0 & c_{44} \end{pmatrix} \begin{pmatrix} \varepsilon_{rr} - \beta_r (T - T_{ref}) \\ \varepsilon_{\varphi\varphi} - \beta_\varphi (T - T_{ref}) \\ \varepsilon_{zz} - \beta_z (T - T_{ref}) \\ \gamma_{rz} \end{pmatrix} \tag{16}$$

where  $\varepsilon_{rr}$ ,  $\varepsilon_{\varphi\varphi}$ ,  $\varepsilon_{zz}$  and  $\gamma_{rz}$  represent the strain components,  $c_{ij}$  are the elastic constants,  $\beta_r$ ,  $\beta_\varphi$  and  $\beta_z$  denote the thermal expansion coefficients in the radial, azimuthal and axial directions, respectively, and  $T_{ref}$  is the reference temperature. The elastic constants  $c_{ij}$  can be obtained by Nguyen et al. (2020). It is assumed that the elastic constants of SiC crystals at high temperature are the same as those at room temperature. The strains are defined as

$$\begin{aligned}
 \varepsilon_{rr} &= \frac{\partial L_r}{\partial r}, \\
 \varepsilon_{\varphi\varphi} &= \frac{L_r}{r}, \\
 \varepsilon_{zz} &= \frac{\partial L_a}{\partial z}, \\
 \gamma_{rz} &= \frac{\partial L_r}{\partial z} + \frac{\partial L_a}{\partial r}
 \end{aligned} \tag{17}$$

where  $L_r$  and  $L_a$  are the displacements in the radial and axial directions, respectively.

The top of the crucible lid is considered to be fixed. The corresponding boundary conditions are

$$L_r = L_a = 0, \quad z = 0. \tag{18}$$

At the central axis, the boundary conditions are as follows

$$L_r = 0, \quad \frac{\partial L_a}{\partial r} = 0, \quad \text{at } r = 0. \tag{19}$$

The growth interface and side surface of SiC crystals are considered as free surfaces, that is

$$\boldsymbol{\sigma} \cdot \mathbf{n} = 0, \quad \text{at } z = -H \text{ or } r = R, \tag{20}$$

where  $H$  and  $R$  are the height and radius of the crystals, respectively.

An alternative indicator for thermal stress commonly used in literature is the von Mises stress. The von Mises stress is defined by

$$\sigma_{\text{Mises}} = \sqrt{\frac{1}{2} \left[ (\sigma_{zz} - \sigma_{rr})^2 + (\sigma_{zz} - \sigma_{\varphi\varphi})^2 + (\sigma_{rr} - \sigma_{\varphi\varphi})^2 + 12r_{rz}^2 \right]} \tag{21}$$

## 2.2 Modelling of crystal growth

The phase field model is employed to model the crystal growth of SiC. It is assumed that thermal property is constant and solid-gas interface is in local equilibrium (Sahoo and Chou, 2016). The temperature distribution of the microscopic growth of SiC crystals is obtained from the macroscopic heat transfer during the sublimation of SiC powder, which is introduced into the phase field equation after the dimensionless treatment of the temperature and used to simulate the crystal growth. The phase field governing equation involving temperature and pressure is (Karma and Rappel, 1998)

$$\tau(n) \frac{\partial \phi}{\partial t} = W_0^2 \nabla \cdot (a_s^2(n) \nabla \phi) + W_0^2 \nabla \cdot \mathcal{N} - (-\phi + \phi^3) - \lambda(1 - \phi^2)^2 (u + A_p(t)), \tag{22}$$

$$\frac{\partial u}{\partial t} = \alpha_0 \nabla^2 u + \frac{1}{2} \frac{\partial \phi}{\partial t}, \tag{23}$$

where  $\tau(\mathbf{n}) = \tau_0 a^2(\mathbf{n})$  is the interfacial kinetic coefficient,  $a_s(\mathbf{n})$  is the interfacial anisotropy for crystal growth,  $W_0$  and  $\tau_0$  are characteristic interface thickness and

relaxation time, respectively,  $\mathcal{N}$  is the anisotropy vector,  $\lambda$  denotes the coupling coefficient with dimensionless undercooling ( $u + A_p(t)$ ),  $\alpha_0$  is thermal diffusion coefficient,  $\alpha_0$  is dimensionless processed in the model, and the expression is  $\alpha_0 = \tilde{\alpha} \cdot W_0^2 / \tau_0$ , where  $\tilde{\alpha}$  represents dimensionless thermal diffusion coefficient.

According to the thin interface analysis, the characteristic interface thickness  $W_0$  and relaxation time  $\tau_0$  are expressed as (Echebarria et al., 2004)

$$W_0 = d_0 \lambda / a_1 \quad (24)$$

$$\tau_0 = d_0^2 a_2 \lambda^3 / (D a_1) \quad (25)$$

where  $d_0$  is the capillary length,  $D$  is thermal diffusivity,  $a_1 = 0.8839$  and  $a_2 = 0.6267$ .

In order to take pressure into account, the way to couple the pressure effects into phasefield equation using methods in Shang et al. (2016) is adopted here.  $A_p(t)$  is the term related to the condensation point caused by pressure according to the Clausius-Clapeyron relationship  $T_c^P = T_c^{P_0} + C_c \Delta P$  (Shang and Han, 2019), where  $\Delta P = P - P_0$  and  $C_c$  is Clapeyron coefficient. From above, we can define  $A_p(t)$  as

$$A_p(t) = \frac{T_c^P - T_c^{P_0}}{L / c_p} = \frac{C_c \Delta P}{L / c_p} \quad (26)$$

Since  $\Delta P = P't$ , where  $P'$  represents pressure variation rates,  $A_p(t)$  is formulated as

$$A_p(t) = \frac{C_c P't}{L / c_p} \quad (27)$$

In this paper, the LB scheme is proposed to solve the phase field equation. The equation for SiC crystal growth is written as (Wang et al., 2020)

$$a_s^2(\mathbf{n}) g_i(\mathbf{x} + e_i \delta x, t + \delta t) = g_i(\mathbf{x}, t) - [1 - a_s^2(\mathbf{n})] g_i(\mathbf{x} + e_i \delta x, t) - \frac{1}{\tau_p(\mathbf{x}, t)} [g_i(\mathbf{x}, t) - g_i^{eq}(\mathbf{x}, t)] + \omega_i Q_p(\mathbf{x}, t) \frac{\delta t}{\tau_0}, \quad (28)$$

where  $g_i$  is the discrete distribution function for phase field,  $e_i$  denotes the discrete velocity,  $w_i$  represents weight coefficient,  $\tau_p$  and  $Q_p$  are the relaxation time for phase transition and source term for crystal growth, and  $g_i^{eq}$  represents equilibrium distribution function for the phase field.

The relaxation time  $\tau_p(\mathbf{x}, t)$  can be computed by

$$\tau_p(\mathbf{x}, t) = \frac{a_s^2(\mathbf{n}) W_0^2}{c_s^2 \delta t} \frac{1}{\tau_0} + \frac{1}{2}. \quad (29)$$

The phase field equilibrium distribution function  $g_i^{eq}$  in anisotropic lattice Boltzmann scheme is defined as (Sun et al., 2019)

$$g_i^{eq}(\mathbf{x}, t) = \omega_i \left[ \phi(\mathbf{x}, t) + \frac{e_i \cdot \mathbf{v}_n}{e_s^2} + \frac{(e_i \cdot \mathbf{v}_n)^2}{2e_s^4} - \frac{|\mathbf{v}_n|^2}{2e_s^2} \right], \quad (30)$$

where  $e_s$  denotes unit lattice sound speed,  $v_n$  represents interface advancing velocity evoked by the surface energy and is expressed as  $v_n = -\mathcal{N}\delta t W_0^2 / (\delta x \tau_0)$ .

The expression for the source term  $Q_p(\mathbf{x}, t)$  associated with crystal growth is defined as

$$Q_p(\mathbf{x}, t) = [\phi - \lambda(\mu + A_p(t))(1 - \phi^2)](1 - \phi^2), \quad (31)$$

where  $u$  is the dimensionless temperature. We have  $u \equiv u(\mathbf{x}, t)$ , and  $u(\mathbf{x}, t) = C_p (T(\mathbf{x}, t) - T_c)/L$  with the specific heat  $C_p$ , the gas temperature  $T(\mathbf{x}, t)$ , the condensation temperature  $T_c$ , and the latent heat  $L$ .

In simulating the SiC gas condensation process at the seed, the D2Q9 modelling (Qian et al., 1992) is applied to discrete the computational domain to ensure its numerical stability and calculation accuracy. The discrete velocities  $e_i$  are defined as

$$[e_i, i = 0, \dots, 8] = \begin{bmatrix} 0, c, 0, -c, 0, c, -c, -c, c \\ 0, 0, c, 0, -c, c, c, -c, -c \end{bmatrix}, \quad (32)$$

where  $c$  is the lattice velocity, and  $c \equiv e\delta x/\delta t$ . The unit lattice sound speed  $e_s$  and the lattice sound speed  $c_s$  are defined as  $e_s = e/\sqrt{3}$  and  $c_s = c\sqrt{3}$ , respectively. Where  $e = 1$ . For D2Q9 modelling, the weight coefficient  $w_i$  are

$$\omega_i = \begin{cases} 4/9, & i = 0 \\ 1/9, & i = 1-4 \\ 1/36, & i = 5-8 \end{cases} \quad (33)$$

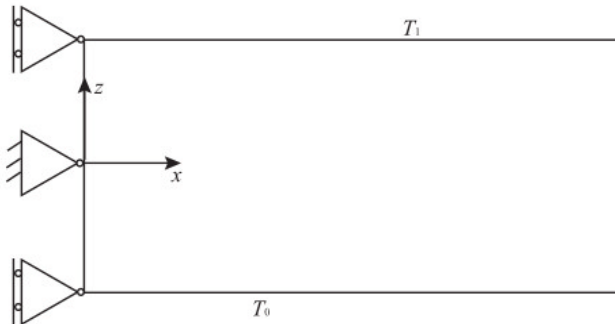
### 3 Results and discussions

#### 3.1 Model validation

##### 3.1.1 Validation of thermal stress model

The thermal stress has a significant effect on crystal quality during crystal growth. Thermal stress distribution of SiC crystals can be obtained by using the displacement-based method. A two-dimensional cantilever beam with uniform temperature variation (Figure 2) has been used to verify the accuracy of the model.

**Figure 2** The schematic diagram of a two-dimensional cantilever beam under linear temperature



For a cantilever beam whose length is much longer than its width, the analytical solution of displacement can be obtained as follows (Hattel and Hansen, 1995)

$$L_x = \alpha_c k_t xz, \quad L_y = \frac{1}{2} \alpha_c k_t (z^2 - x^2), \tag{34}$$

where  $L_x$  is horizontal displacement, and  $L_y$  denotes vertical displacement.

Then, the expression of the combined displacement  $L_{xy}$  can be written as follows

$$L_{xy} = \frac{1}{2} \alpha_c k_t (z^2 + x^2), \tag{35}$$

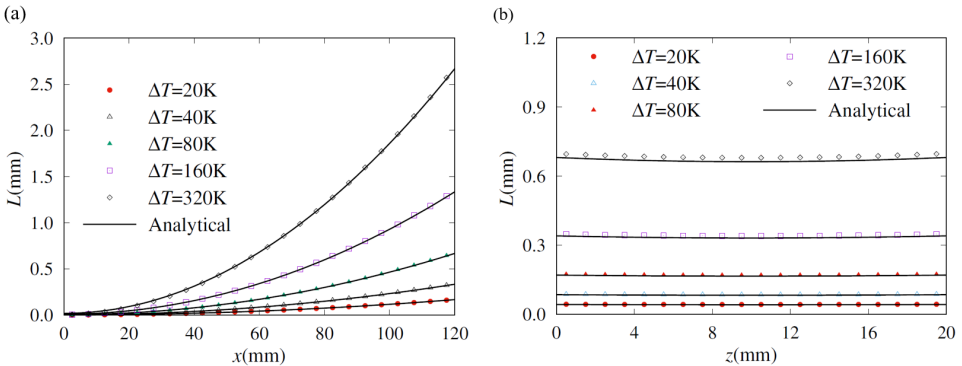
where  $\alpha_c$  is the coefficient of thermal expansion, and  $k_t$  is the ratio of temperature difference to height when the temperature changes linearly, the expression of  $k_t$  is

$$k_t = \Delta T / h_t \tag{36}$$

where  $\Delta T$  is temperature difference between upper and lower levels, and  $h_t$  is the height of the cantilever beam.

The size of cantilever beam used in this simulation is 120×20×2 mm, in which the y-direction is 2 mm, compared with the length and height, the dimension in this direction is negligible. Therefore, it can be simplified to a two-dimensional model. The results are shown in Figure 3. It can be seen that the simulation results are in good agreement with the analytical solution, indicating the accuracy of the thermal stress model.

**Figure 3** Displacement under different conditions of  $\Delta T$  and positions: (a)  $z = 0$  and (b)  $x = 60\text{mm}$ (see online version for colours)



### 3.1.2 Validation of modelling of crystal growth

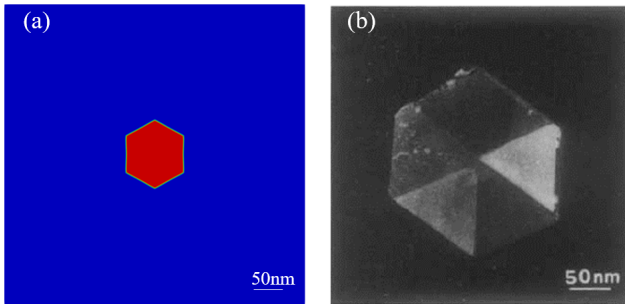
The crystal morphology obtained by the simulation is validated. In the present simulation, the computational domain is divided into a uniform square lattice of 1000×1000. The lattice size is set as  $\delta x/W_0 = 0.008$ , the time interval is set as  $\delta t = 0.005\tau_0$ . The initial dimensionless temperature is set to be  $u = -0.1$ , the pressure  $P$  is set as 1000 Pa and  $P' = 0$ . The anisotropic strength  $\varepsilon_1 = 0.5$  is used, and the simulation parameters are listed in Table 1. At the initial moment, a round seed of radius  $R$  is placed in the centre of the domain, the crystal nucleus grows under dimensionless temperature and pressure.

Figure 4 shows the comparison of the crystal morphology between the simulated and experimental result, which is in good agreement.

**Table 1** Simulation parameters of SiC crystals in the present simulation

<i>Symbol</i>	<i>Parameters</i>	<i>Value</i>	<i>Unit</i>
$c_p$	Specific heat capacity	1200	J/(kg·K)
$L$	Latent heat	$1.2 \times 10^6$	J/kg
$T_c$	Condensation temperature	2300	K
$d_0$	Capillary length	$3 \times 10^{-7}$	m
$\alpha_0$	Thermal diffusion coefficient	$2 \times 10^{-10}$	m <sup>2</sup> /s
$W_0$	Diffuse interface width	$1.25 \times 10^{-7}$	m
$\tau_0$	Relaxation time	$1.47 \times 10^{-4}$	s

**Figure 4** Comparison of the crystal morphology: (a) the simulated result under the conditions of  $u = -0.06$  and  $t = 0.03$  s, (b) the experiment result (see online version for colours)



Source: Sato et al. (1984)

### 3.2 Simulation of convective heat transfer and thermal stress

In the preparation of SiC crystal, the SiC powder is heated and sublimed into gas, transported to the surface of seed under the action of temperature gradient, and then crystallised on the surface of seed. Temperature plays an important role in this process. Higher temperature will cause the powder to sublimate too fast, and will also increase the surface temperature of seed, so that gas cannot condense on the surface of seed crystal. Lower temperature leads to incomplete sublimation of powder and low efficiency of SiC crystal preparation. So it is of great significance to study the internal temperature evolution law of SiC crystal growth device. During the process of crystal growth, the current and coil position have an important effect on the ambient temperature inside the crystal growth device. In this paper, the current and coil position are simulated to analyse their influence on the ambient temperature inside the growth device. Thermal stress plays a crucial role in the generation of propagation defects in SiC ingots. If the thermal stress becomes very high, it can lead to crystal cracking. As the SiC crystal continues to grow, the free energy of the crystal deposited on the seed continues to increase. In order to maintain a stable state of the system, various defects will appear in the crystals to release the thermal stress in the growth system. Therefore, it is of great significance to study the distribution of thermal stress in crystals.

A device for SiC crystal growth with a 13-turn coil in PVT is selected for the study, in which induction current is 100 A, the frequency is 30 kHz and the initial distance between the surface of SiC powder and the seed is 60 mm. Some of the physical properties of materials related to heat transfer in the simulations are shown in Table 2.

**Table 2** Physical properties of materials in SiC sublimation growth process

<i>Symbol</i>	<i>Physical parameters</i>	<i>Value</i>	<i>Unit</i>
$\kappa_1$	Thermal conductivity of susceptor and crucible	150	W/(m·K)
$\kappa_2$	Thermal conductivity of insulation	0.3	W/(m·K)
$\kappa_3$	Thermal conductivity of SiC powder	18	W/(m·K)
$\epsilon_0$	Surface emissivity of susceptor and crucible	0.9	–
$\rho_1$	Susceptor and crucible density	1950	kg/m <sup>3</sup>
$\rho_2$	Insulation density	120	kg/m <sup>3</sup>
$\rho_3$	SiC powder density	1700	kg/m <sup>3</sup>
$\sigma_1$	Electrical conductivity of coil	$6 \times 10^7$	S/m
$\sigma_2$	Electrical conductivity of susceptor and crucible	3000	S/m
$\sigma_3$	Electrical conductivity of insulation	0	S/m

### 3.2.1 Distribution of magnetic and temperature

Figure 5 shows the distribution of the magnetic potential vector  $A$  in the SiC sublimation growth process. The magnetic potential vector  $A$  reaches the maximum around the coil, the contours emanate from the coil and concentrate in the outer region of the susceptor. A large amount of energy is generated by eddy current in the susceptor within a small skin depth due to the susceptor with a high conductivity, allowing very little energy generated in the parts inside the crucible (like the seed and powder). As a result, the eddy current is reduced at the inner surface of the crucible, causing a non-uniform heat distribution.

**Figure 5** The distribution of magnetic potential vector  $A$  in the SiC sublimation growth process (see online version for colours)

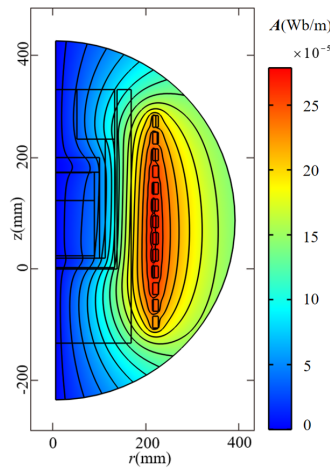
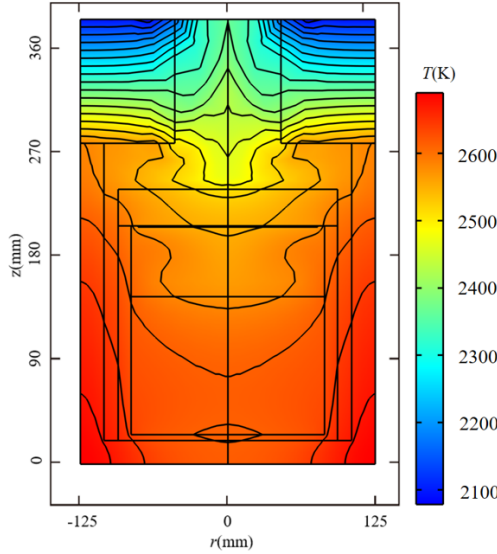


Figure 6 shows the temperature distribution of the SiC sublimation growth process. The highest temperatures are located in the middle, low regions of the inner crucible wall and susceptor. The temperature decreases gradually along the axial direction which is content with the requirement of SiC crystal growth.

**Figure 6** The distribution of temperature in the SiC sublimation growth process (see online version for colours)



### 3.2.2 Distribution of thermal stress

The stress distribution in the seed is calculated in the model. Here, the presence of polycrystal is considered to be negligible, the seed periphery is free of traction and the seed-mounting surface is totally rigid. The thermal conductivity of crucible and seed are  $1.3 \times 10^5/T$  (W/(m K)) and  $4.5 \times 10^5/T^{1.29}$  (W/(m K)), respectively. The relevant physical parameters of the crucible and the seed are listed in Table 3.

**Table 3** Physical parameters in the present simulation

Symbol	Parameters	Crucible	Seed	Unit
$\rho$	Density	1950	3200	kg/m <sup>3</sup>
$c_p$	Atmospheric heat capacity	710	1200	J/(kg K)
$\mu$	Poisson's ratio	0.15	0.3	1
$E$	Young's modulus	11.5	430	GPa
$G$	Shear modulus	4.81	163	GPa
$\beta$	Thermal expansion coefficient	$1.6 \times 10^{-5}$	$4.5 \times 10^{-6}$	1/K

Figure 7(a) shows the distribution of stress component  $\sigma_{rr}$  in the seed. It can be seen that the maximum absolute value  $\sigma_{rr}$  appears at the upper edge of seed, this is due to the bonding and the difference of thermal expansion coefficient  $\beta_r$  between the seed and the crucible lid. Figure 7(b) gives the distribution of  $\sigma_{\varphi\varphi}$ , which shows a similar distribution

pattern as  $\sigma_{rr}$ . They are both compressive stresses toward the growth front, and the radial variations of these two stress components are higher than the axial ones.

**Figure 7** The distribution of thermal stress in the seed: (a)  $\sigma_{rr}$ , (b)  $\sigma_{\phi\phi}$ , (c)  $\sigma_{zz}$  and (d)  $\tau_{rz}$  (see online version for colours)

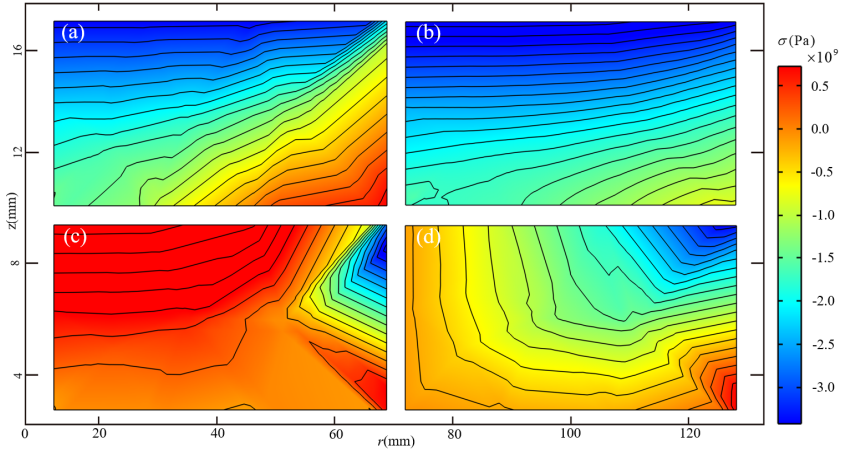
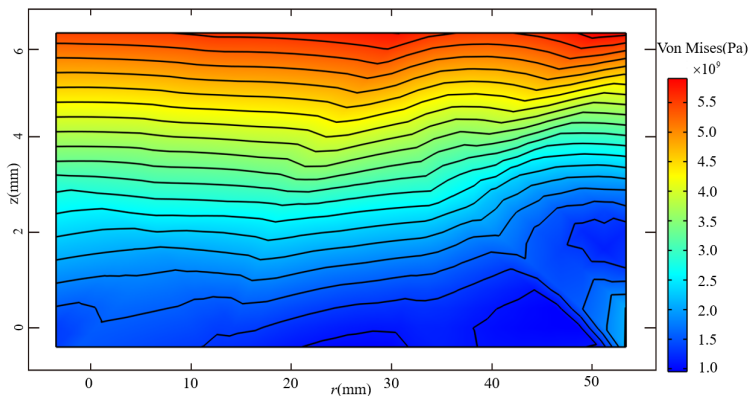


Figure 7(c) shows that  $\sigma_{zz}$  is tensile close to the symmetry axis of the seed and compressive near the seed periphery. The result shows that the maximum absolute value of  $\sigma_{zz}$  is near the seed periphery. The axial variation of  $\sigma_{zz}$  is much larger than the radial variation.

From Figure 7(d) we can see that the shear stress  $\tau_{rz}$  has small absolute values near the symmetry axis, the absolute value of  $\tau_{rz}$  decreases along the growth direction, which can be attributed to stress and thermal boundary conditions. The maximum absolute value of  $\tau_{rz}$  is found near the upper edge of seed, which is due to the attachment of rigid seed resulting in high shear stress.

Figure 8 shows the distribution of von Mises stress in the seed. The von Mises stress is relatively low in the growth front. The axial variation of von Mises stress is higher than the radial variation and the maximum occurs near the upper part of the seed. The maximum von Mises stress occurs near the upper part of the seed.

**Figure 8** The distribution of von Mises stress in the seed (see online version for colours)



### 3.2.3 Effect of current on temperature

During crystal growth, it is usually necessary to adjust the current to change the temperature to obtain the high quality crystals. Set the frequency condition of 30 kHz in the simulations. Figure 10 shows the temperature of the central axis of the sublimation growth process and the crystal growth surface (the locations are shown in Figure 9) change with the currents after the SiC sublimation growth reaches thermal equilibrium. The axial temperature distribution curves inside the growth environment and the radial temperature distribution curves of growth interface are almost parallel under different currents, which indicate that changing the current changes the overall temperature inside the growth environment, but has little effects on the axial temperature gradient in the growth environment and the radial temperature gradient of the crystal growth surface.

**Figure 9** The diagram of different positions of the internal environment of SiC crystal growth device (see online version for colours)

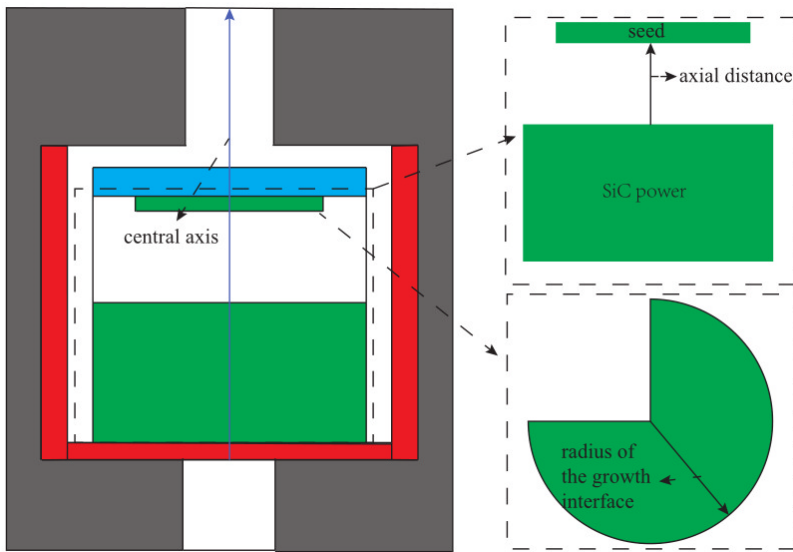
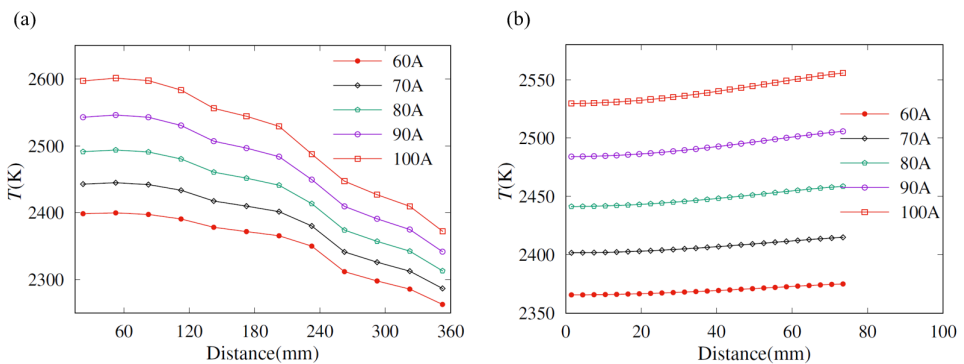


**Figure 10** The temperature distribution with currents under different positions: (a) central axis distance in the sublimation growth process and (b) radius of growth interface (see online version for colours)

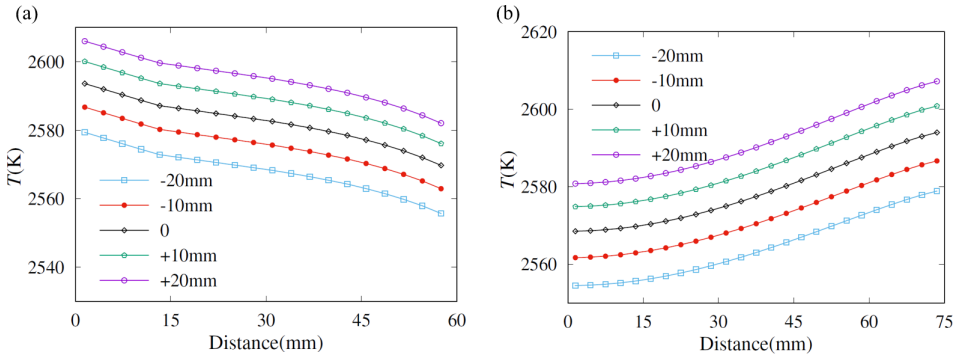


### 3.2.4 Effect of coil position on temperature

By moving the induction coil vertically (upward or downward), the temperature difference between the powder and the seed can be changed. In order to study the influences of the coil positions on the temperature, the following cases are taken for comparative study. It is specified that when the centre of the coil is parallel to the bottom of the susceptor, the position is recorded as 0, the centre position of the coil above the bottom of the susceptor is recorded as positive and below is negative. Coil positions are selected as -20 mm, -10 mm, 0, +10 mm and +20 mm for study in the present simulation.

Given the current and frequency of growth device are 100 A and 30 kHz, respectively. As seen in Figure 11(a), the axial temperature gradient between the sublimation surface of the SiC powder and the crystal growth surface decreases gradually with the increase of the coil position. From Figure 11(b), the temperature of the SiC crystal growth surface increases with the upward movement of the coil position.

**Figure 11** The temperature distribution under different positions: (a) axial distance from the SiC powder to the surface of the seed and (b) radius of the growth interface (see online version for colours)



The upward shift of the coil can increase the temperature of the SiC crystal growth surface, which not only contributes to increase the crystal growth rate, but reduces the axial temperature gradient, in turn decreases the crystal growth rate. As can be seen from Figure 11(b), when the positions of coil center are located at -20 mm and +20 mm, the crystal surface temperature changes by about 60 K, and the temperature increment of the crystal surface is small compared with the crystal surface temperature. Therefore, relative to the crystal temperature change, the axial temperature gradient in the growth environment is the main factor affecting the crystal growth rate.

### 3.3 Simulation of crystal growth

The condensation rate of SiC gas can significantly affect the quality of crystal growth. Slow sublimation speed leads to inability to meet the needs of industrial production, and fast growth speed can lead to significant expansion defects in the grown crystals. Therefore, it is very important to study the crystal growth rate in the process of gas condensation. Temperature and pressure play an important role in the process of SiC gas sublimation, so the effects of temperature and pressure on crystal growth are studied in this paper.

In order to investigate the SiC crystal growth under dimensionless temperature and pressure variation rates, a series of simulations have been studied. Firstly, the morphology of the SiC crystals is investigated. Initially, a round seed of radius  $R$  is placed in the centre of the domain of size  $L \times L$ . Figure 12 shows the numerical result of crystal growth with time. The seed grows along the radial epitaxial direction, and eventually becomes a large hexagon.

**Figure 12** The morphological evolution of SiC crystals with times at  $u = -0.04$  and  $P' = 0$ : (a)  $t = 0.01$  s; (b)  $t = 0.02$  s and (c)  $t = 0.03$  s (see online version for colours)

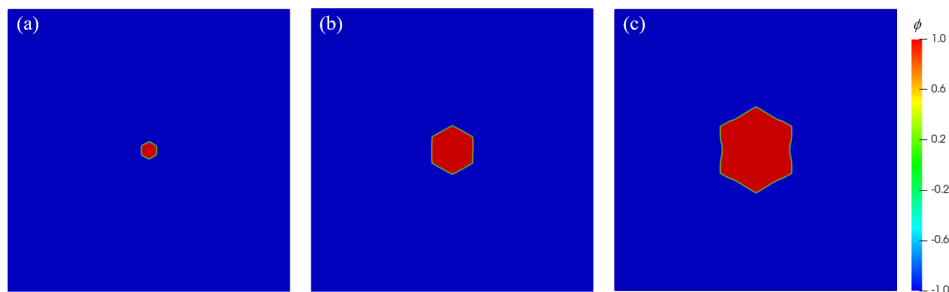
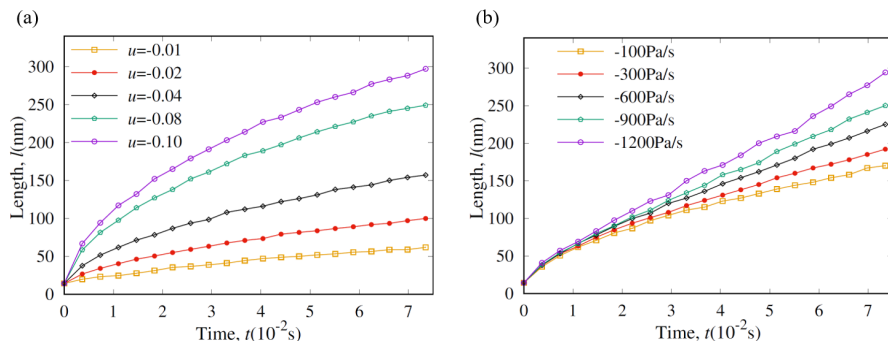


Figure 13 shows the influences of dimensionless temperature and pressure variation rates on the SiC crystal growth. Figure 13(a) shows the crystal growth of SiC under different dimensionless temperature  $u$  at different times, it can be observed that dimensionless temperature  $u$  affects the growth rates of crystal largely. The crystal growth rate is gradually accelerated as the absolute of  $u$  increases and the crystal size is much larger for the same time with  $u = -0.10$  than for  $u = -0.01$ . Figure 13(b) shows the growth of SiC crystals with time under different drop rates of pressure when  $u$  is  $-0.04$ . It can be inferred that the growth rate of crystals at low absolute of pressure drop rate is very different from that at high absolute of pressure drop rate. When the absolute of pressure drop rate is higher, the growth of crystal is promoted more. This is mainly because the greater the absolute of pressure drop rate, the sublimation rate of SiC powder will also increase, making the supersaturation of the gas phase on the growth surface of SiC crystal increase, and then increase the growth rate of SiC crystal. In summary, the crystal growth rates can be increased by improving the absolute of dimensionless temperature and pressure drop rates.

**Figure 13** The growth of SiC crystals with times under different dimensionless temperature (a) and pressure drop rates (b) (see online version for colours)



## 4 Conclusion

A LB-PF model is proposed to investigate crystal growth of SiC, which includes the convective heat transfer, thermal stress generation and crystal growth. The model is validated by simulation of thermal stress generation in a cantilever beam, then, the crystal growth by simulation is in good agreement with the experimental observation. The results show that the present model can be used to simulate the growth of crystals and guide the experimental preparation of SiC crystals.

The temperature and magnetic distribution in the growth environment are calculated, the results of von Mises show that the stress concentration in the upper part of the crystals. Changing the current and coil position have small influence on the radial temperature gradient of the crystal growth surface. The crystal growth with different pressure variation rates and dimensionless temperature is investigated, the results show that the crystal growth rates can be increased by improving the absolute of dimensionless temperature and pressure drop rates.

## References

- Ariyawong, K., Chatillon, C., Blanquet, E., Dedulle, J.M. and Chaussende, D. (2015) 'Assessment of SiC crystal chemistry during the PVT growth process: coupled numerical modeling and thermodynamics approach', *Materials Science Forum*, Vol. 821, Trans Tech Publ., pp.96–99.
- Chaussende, D., Eid, J., Mercier, F., Madar, R. and Pons, M. (2009) 'Nucleation and growth of 3c-SiC single crystals from the vapor phase', *Materials Science Forum*, Vol. 615, Trans Tech Publ, pp.31–36.
- Chen, Q-S., Yan, J-Y. and Prasad, V. (2007) 'Application of flow-kinetics model to the PVT growth of SiC crystals', *Journal of Crystal Growth*, Vol. 303, No. 1, pp.357–361.
- Chen, Q-S., Zhang, H., Prasad, V., Balkas, C., Yushin, N. and Wang, S. (2001) 'Kinetics and modeling of sublimation growth of silicon carbide bulk crystal', *Journal of Crystal Growth*, Vol. 224, Nos. 1–2, pp.101–110.
- Chen, X., Nishizawa, S-i. and Kakimoto, K. (2010) 'Numerical simulation of a new SiC growth system by the dual-directional sublimation method', *Journal of Crystal Growth*, Vol. 312, No. 10, pp.1697–1702.
- Echebarria, B., Folch, R., Karma, A. and Plapp, M. (2004) 'Quantitative phase-field model of alloy solidification', *Physical Review E*, Vol. 70, No. 6, pp.061604.
- Geiser, J. and Irle, S. (2011) 'Macro-and microsimulations for a sublimation growth of SiC single crystals', *Mathematical Problems in Engineering*, Vol. 2009, No. 2, p.716104.
- Ha, M-T. and Jeong, S-M. (2022) 'A review of the simulation studies on the bulk growth of silicon carbide single crystals', *Journal of the Korean Ceramic Society*, Vol. 59, No. 2, pp.153–179.
- Hattel, J. and Hansen, P. (1995) 'A control volume-based finite difference method for solving the equilibrium equations in terms of displacements', *Applied Mathematical Modelling*, Vol. 19, No. 4, pp.210–243.
- Karma, A. and Rappel, W-J. (1998) 'Quantitative phase-field modeling of dendritic growth in two and three dimensions', *Physical Review E*, Vol. 57, No. 4, p.4323.
- Kim, J.G., Kim, Y.H., Lee, K.M., Sohn, H.C. and Choi, D.J. (2012) 'Changes in thermal conductivity and bandgap of SiC single crystals in accordance with thermal stress', *Thermochimica acta*, Vol. 542, pp.6–10.
- Kimoto, T. (2016) 'Bulk and epitaxial growth of silicon carbide', *Progress in Crystal Growth and Characterization of Materials*, Vol. 62, No. 2, pp.329–351.

- Li, Y., Hu, Y. and Wu, L. (2011) 'Numerical simulation analysis of temperature field on silicon carbide synthesis furnace', *Materials Science Forum*, Vol. 686, pp.494–500.
- Liu, X., Shi, E-W., Song, L-X. and Chen, Z-Z. (2008) 'Effects of graphitization of the crucible on silicon carbide crystal growth', *Journal of Crystal Growth*, Vol. 310, No. 19, pp.4314–4318.
- Ma, R-H., Zhang, H., Ha, S. and Skowronski, M. (2003) 'Integrated process modeling and experimental validation of silicon carbide sublimation growth', *Journal of Crystal Growth*, Vol. 252, No. 4, pp.523–537.
- Nguyen, B.D., Rausch, A.M., Steiner, J., Wellmann, P. and Sandfeld, S. (2020) 'On the importance of dislocation flow in continuum plasticity models for semiconductor materials', *Journal of Crystal Growth*, Vol. 532, pp.125414.
- Qian, Y-H., d'Humières, D. and Lallemand, P. (1992) 'Lattice BGK models for Navier-Stokes equation', *Europhysics letters*, Vol. 17, No. 6, pp.479.
- Sahoo, S. and Chou, K. (2016) 'Phase-field simulation of microstructure evolution of Ti-6Al-4V in electron beam additive manufacturing process', *Additive Manufacturing*, Vol. 9, pp.14–24.
- Sato, H., Otsuka, N., Liedl, G. and MANSOUR, S. (1984) 'Hexagonal  $\beta$ -SiC particles', *Journal of the American Ceramic Society*, Vol. 67, No. 2, pp.103–105.
- Shang, S. and Han, Z. (2019) 'In situ observation and phase-field simulation on the influence of pressure rate on dendritic growth kinetics in the solidification of succinonitrile', *Journal of Materials Science*, Vol. 54, pp.3111–3124.
- Shang, S., Guo, Z. and Han, Z. (2016) 'On the kinetics of dendritic sidebranching: A three dimensional phase field study', *Journal of Applied Physics*, Vol. 119, No. 16, pp.164305.
- Su, J., Chen, X. and Yuan, L. (2014) 'Numerical design of induction heating in the pvt growth of Si crystal', *Journal of Crystal Growth*, Vol. 401, No. sep.1, pp.128–132.
- Sun, D., Xing, H., Dong, X. and Han, Y. (2019) 'An anisotropic lattice Boltzmann–phase field scheme for numerical simulations of dendritic growth with melt convection', *International Journal of Heat and Mass Transfer*, Vol. 133, pp.1240–1250.
- Tokuda, Y., Kojima, J., Hara, K., Tsuchida, H. and Onda, S. (2014) '4h-SiC bulk growth using high-temperature gas source method', *Materials Science Forum*, Vol. 778, Trans Tech Publ, pp.51–54.
- Wang, X., Sun, D., Xing, H., Han, Y., Liu, Y. and Wang, J. (2020) 'Numerical modeling of equiaxed crystal growth in solidification of binary alloys using a Lattice Boltzmann-finite volume scheme', *Computational Materials Science*, Vol. 184, pp.109855.
- Wellmann, P.J. (2018) 'Review of SiC crystal growth technology', *Semiconductor Science and Technology*, Vol. 33, No. 10, pp.103001.
- Yan, J-Y., Chen, Q-S., Jiang, Y-N. and Zhang, H. (2014) 'Improvement of the thermal design in the SiC PVT growth process', *Journal of Crystal Growth*, Vol. 385, pp.34–37.
- Yang, C., Liu, G., Chen, C., Hou, Y., Xu, M. and Zhang, Y. (2018a) 'Numerical simulation of temperature fields in a three-dimensional SiC crystal growth furnace with axisymmetric and spiral coils', *Applied Sciences*, Vol. 8, No. 5, p.705.
- Yang, M.C., Chen, Z.M., Feng, X.F., Lin, S.H., Ke, L.I., Liu, S.J. and Liu, Z.F. (2012) 'Effect of the growth interface shape on the thermoelastic stresses in SiC crystal prepared by PVT technique', *Journal of Synthetic Crystals*, Vol. 41, No. 1, pp.24–27.
- Yang, N., Song, B., Wang, W. and Li, H. (2022) 'Control of the temperature field by double induction coils for growth of large-sized SiC single crystals via the physical vapor transport technique', *CrystEngComm*, Vol. 24, No. 18, pp.3475–3480.
- Yang, Y.B., Wang, J. and Wang, Y.M. (2018b) 'Thermal stress simulation of optimized sic single crystal growth crucible structure', *Journal of Crystal Growth*, Vol. 504, pp.31–36.